

---

# MODEL DISCOVERY FOR DYNAMICAL SYSTEMS WITH COMPLEX-VALUED PRODUCT UNITS

---

**Martin Brückmann, Babette Dellen, Uwe Jaekel**

Department of Mathematics, Informatics, and Technology, RheinAhrCampus Remagen  
University of Applied Sciences Koblenz  
Joseph-Rovan-Allee 2, 53424 Remagen, Germany  
{brueckmann, dellen, jaekel}@hs-koblenz.de

## ABSTRACT

Discovering the governing equations of a dynamical system from observed trajectories provides deeper insight into its structure than mere prediction of future states. We present a data-driven approach to model discovery based on complex-valued product-unit networks, in which each unit represents a complex monomial and the network output is a sparse linear combination of such monomials. In contrast to established library-based methods such as SINDy, our approach does not require a predefined set of candidate functions: the relevant monomials, including those with fractional or negative exponents, are learned directly from data. Across four chaotic benchmark systems (Lorenz63, Lorenz84, the Four-Wing attractor, and a fractional variant of Lorenz63), we recover the exact governing equations in 90% of trials for the first three systems, and in 70–90% of trials for the fractional case, using at least 3000 training points. Applied to real-world human-gait accelerometer signals, the model produced stable trajectories with bounded prediction errors, corresponding to an RMSE of approximately 12–14% of the signal amplitude range over a test horizon three times longer than the training interval, demonstrating its potential for high-dimensional systems in which analytic equations are unavailable.

## 1 Introduction

It is well known that highly complex patterns and even chaos in dynamical systems can emerge from comparatively simple governing equations. For example, the chaotic dynamics of the Lorenz attractor [1, 2], originally serving as a model for weather phenomena, arises from three sparse nonlinear polynomial equations, consisting of monomials that couple the main variables of the system by multiplication. The recovery of the accurate algebraic structure of the leading monomials driving the dynamical system is highly valuable for gaining a better understanding of the properties of the system, such as dynamic stability and interaction of variables, as well as further theoretical insights. Examples of real-world data originating from dynamical systems are physiological time series, such as human-gait accelerometer data, or EEG [3] and ECG [4] data, but also machine vibrations in predictive maintenance [5]. A major challenge in identifying the relevant monomials, or more generally terms with fractional or negative exponents, for high-dimensional systems is the vast, potentially infinite, number of candidate terms to be explored. Since this number grows exponentially with the input dimension, exhaustive search quickly becomes intractable.

In recent years, several neural-network-based approaches have been proposed to learn sparse polynomial representations from data that have shown promising results. First-order input couplings were implemented for a reservoir-computing approach applied to the problem of forecasting the behavior of the Lorenz system [6]. Higher-order couplings have also been used in the SINDy approach to model nonlinear dynamical systems [7]. Using a preset candidate library of monomials, the active candidates are determined using sparse regression.

Wang and Li (2024) have recently proposed the dynamical-system deep-learning (DSDL) model to predict chaotic time series, which is based on a state-space reconstruction (SSR) technique and can, unlike many traditional deep-learning approaches, also infer important variables and high-degree interactions of the system [8]. Their architecture was shown to be effective with noisy data [9] and also delivered promising results for partial differential equations [10].

Another notable approach is symbolic regression, which aims to find short mathematical expressions that describe the underlying data, typically making use of genetic programming or the usually faster FFX algorithm. The latter utilizes a large candidate set of combinations of nonlinear functions to subsequently collect Pareto optimal expressions that trade off error and the number of terms in the representation [11, 12].

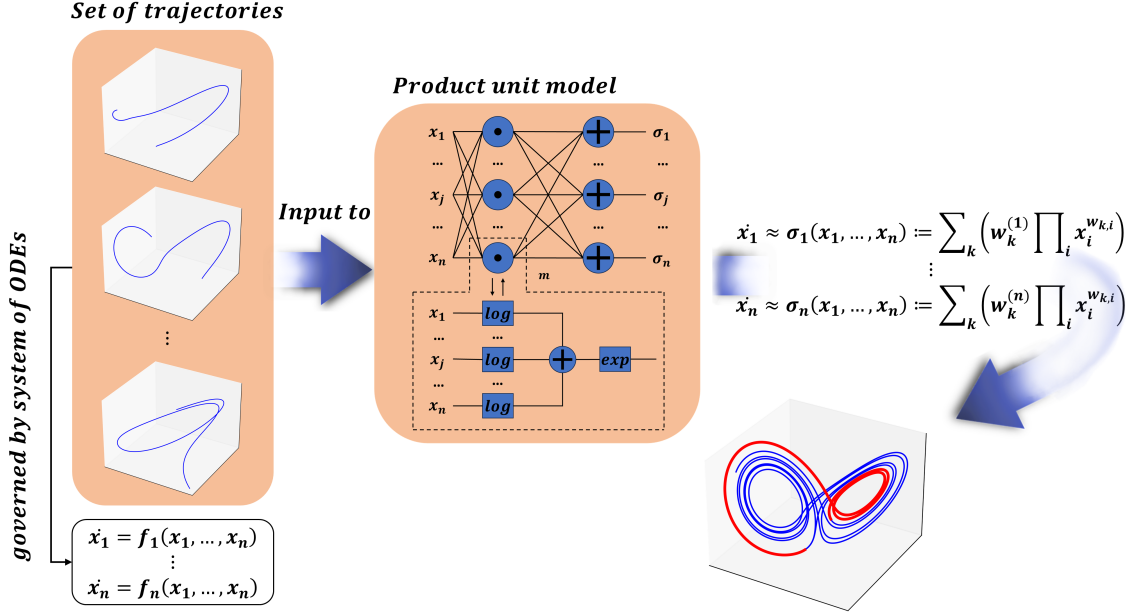


Figure 1: General approach for systems following differential equations: We assume knowledge of a time series of training trajectories in phase space, consisting of points and the numerical values of their time derivatives. If values for the derivatives are not directly available, we assume that they can be approximated numerically. The data are assumed to be subject to a system of ordinary differential equations. By comparing evaluations of the true equations at these points with derivatives obtained from the model, the product-unit model fits the inputs to linear combinations of monomials to approximate the original equations, i.e., we learn the right-hand side (RHS) of equations  $\dot{x}_j$ . Furthermore, the derived equations permit prediction of future system states. The stability of trajectories generated from the model's equations can be assessed using the effective prediction time (EPT), which indicates the point at which the predicted trajectory diverges from the true trajectory.

However, these approaches are limited because of their use of predefined candidate functions or monomials, restricting the number of nonlinear function classes that can be represented by the model, which is particularly severe for high-dimensional problems. Therefore, we follow a different approach. Product units are neural network units that can be trained to take the form of any monomial or even algebraic terms containing fractional or negative exponents [13, 14, 15, 16], but which can be difficult to train. Recently, it could be shown that complex-valued product unit networks can successfully learn sparse approximations of real-valued functions from real data and outperform classical multi-layer perceptrons in extrapolation tasks [17]. The complex-valued product-unit network operates fully in the complex domain, meaning that its inputs, outputs, and weights are complex-valued, which distinguishes it from previous approaches. Training of this network could be achieved by standard gradient descent using a loss defined for complex-valued outputs. In this work, we use complex-valued product unit networks to learn the governing equations of dynamical systems directly from observed trajectories of the system.

Here, we focus on dynamical systems with a moderate, but unknown number of multiplicative couplings of fractional power laws in the dynamical variables. Note that this includes the possibility of approximating other non-linear couplings in terms of Taylor- or Laurent expansions. A major challenge in the identification of the dominant monomial terms lies in the large number of possible couplings, which grows exponentially with the number of variables. Since the required leading terms of the sparse polynomial as well as potentially fractional exponents in our approach are learned from the data directly without using a candidate library, the problem of complexity-of-choice is avoided.

To determine its aptitude in extracting the governing equations of a dynamical system from state trajectories, the proposed method is tested on some standard benchmark problems, i.e., the Lorenz63 attractor, Lorenz84 and a Four Wing system. Furthermore, a modified instance of Lorenz63 is investigated, which now includes a fractional exponent

in the third equation. We finally apply the product-unit model to real-world human-gait patterns in order to learn a mathematical representation of human gait.

## 2 Methods

This section introduces the complex-valued product-unit model, the benchmark dynamical systems used for evaluation, and evaluation measures. A general overview of the approach can be seen in Fig. 1: The model is trained on a set of simulated trajectories (discrete points and their derivatives) to learn the precise terms of the underlying differential equations. Subsequently, the identified equations and the stability of their predictions over time are assessed.

### 2.1 Complex-Valued Product-Unit-Network Model

The model consists of nonlinear units that compute products of their inputs according to  $\prod_{i=1}^n x_i^{w_i}$  with complex-valued weights  $w_i$  [17]. In practice, these product units are implemented by concatenating summation units with logarithmic and exponential activation functions defined in the complex domain (Fig. 1), such that

$$\prod_{i=1}^n x_i^{w_i} = \exp\left(\sum_{i=1}^n w_i \log x_i\right). \quad (1)$$

The complex-valued formulation enables the model to handle negative and complex inputs naturally. However, inputs cannot be zero, but this constraint rarely poses practical limitations [17].

The resulting complex-valued units are subsequently supplied to a summation layer, so that an equation is represented as a linear combination of (generalized) monomials by

$$\hat{f}(x_1, \dots, x_n) := \sum_{k=1}^m c_k \prod_{i=1}^n x_i^{w_{k,i}}, \quad (2)$$

where  $c_k \in \mathbb{C}$  is the coefficient of the  $k$ -th monomial and  $w_{k,i} \in \mathbb{C}$  is the exponent of variable  $x_i$  in that monomial, following [17]. The output of this function is a complex number and both the real and the imaginary part are supplied to the loss function.

For a system with multiple equations, we use a product-unit model that realizes one sum per equation. For a set of three ordinary differential equations, as it is the case for the benchmark problems (Sec. 2.2), we learn the right-hand side (RHS) of the equations

$$\begin{aligned} \dot{x} &= f_x(x, y, z), \\ \dot{y} &= f_y(x, y, z), \\ \dot{z} &= f_z(x, y, z), \end{aligned} \quad (3)$$

directly, so that each function  $f_{v \in \{x, y, z\}}$  is represented by a weighted sum of product units, denoted  $\hat{f}_v$ . For the real-world human gait signals considered in this work, three-dimensional acceleration measurements likewise allow the dynamics to be captured by three equations. However, in the latter case we predict the future directly from past states.

For example,  $f_x(x, y, z) = 5x^2y^3 + xz^{0.1} - 4$  can be rewritten in a normalized form by expressing each term as a product of powers of the variables  $x, y$  and  $z$ :

$$5x^2y^3z^0 + 1x^1y^0z^{0.1} + (-4)x^0y^0z^0.$$

Thus, the formula can be represented by three product units.

Equations of dynamical systems may share monomials, for instance the term  $xy$  appears in both  $\dot{y}$  and  $\dot{z}$  of the Lorenz84 system. To accommodate such shared terms, we allow the product-unit layer to be fully connected with the summation-unit layer, leading to the mathematical model given by Eq. 2.

The model is implemented in PyTorch [18], using the formulation in Eq. 1, where each product unit is implemented as a complex-valued linear layer with bias in the logarithmic domain, followed by an exponential activation.

### 2.2 Benchmark systems

For benchmarking, we simulate the trajectories of several three-dimensional dynamical systems using numerical methods. Therefore, we have access to numerical approximations of the state variables and their time derivatives. From

these discrete observations, our goal is to recover the underlying differential equations that govern the system. We then compare the parameters and structure of the discovered model with the true system. Using this model, we approximate trajectory predictions using numerical methods.

We first consider three known examples of chaotic dynamical systems of first-order ordinary differential equations to show the general applicability of the model in this regard: The Lorenz63 system [1], as well as Lorenz84 [19], and a Four-Wing chaotic attractor introduced by Wang et al. (2009) [20]. The systems vary in the minimum number of product units required to represent their terms, which makes them good candidates for benchmarking. The system Lorenz63 requires at least five product units, Four Wing requires six, and Lorenz84 requires eight. Furthermore, a modified version of Lorenz63 is considered which includes a term with a fractional exponent.

The Lorenz63 system, originally proposed by E. N. Lorenz in 1963, consists of a set of three coupled ordinary differential equations [1],

$$\begin{aligned}\dot{x} &= \sigma(-x + y), \\ \dot{y} &= -xz + \rho x - y, \\ \dot{z} &= xy - \beta z.\end{aligned}\tag{4}$$

Parameters are typically chosen as  $\sigma = 10$ ,  $\rho = 28$  and  $\beta = 2.667$ .

Lorenz84 is defined by the governing equations

$$\begin{aligned}\dot{x} &= -y^2 - z^2 - ax + aF, \\ \dot{y} &= xy - bxz - y + G, \\ \dot{z} &= bxy + xz - z,\end{aligned}\tag{5}$$

where  $a = 0.25$ ,  $b = 6$ ,  $F = 16$ , and  $G = 3$  [19].

We further use a butterfly attractor (Four Wing model) [20] with parameters  $a = 0.2$ ,  $b = -0.01$ ,  $c = 1$ ,  $d = -0.4$ ,  $e = -1.0$ ,  $f = -1$ , and equations

$$\begin{aligned}\dot{x} &= ax + cyz, \\ \dot{y} &= bx + dy - xz, \\ \dot{z} &= ez + fxy.\end{aligned}\tag{6}$$

These systems contain only exponents strictly limited to nonnegative integer values. Therefore, another system of ODEs is proposed that is a slightly modified version of Lorenz63 but has a fractional exponent:

$$\begin{aligned}\dot{x} &= \sigma(-x + y), \\ \dot{y} &= -xz + \rho x - y, \\ \dot{z} &= xy - \beta z^\eta.\end{aligned}\tag{7}$$

The parameters are set to  $\sigma = 35$ ,  $\rho = 28$ ,  $\beta = 3$  and  $\eta = 0.5$ . The attractor is shown in Fig. 2 and is referred to as *Lorenz\_Fract* in the following. Note that for negative  $z$ ,  $z^\eta$  with  $\eta = 0.5$  becomes complex. Since our model operates in the complex domain, this poses no fundamental obstacle; however, for the numerical generation of training data we restrict trajectories to the positive orthant (see Sec. 2.4) to ensure stable RK4 integration.

### 2.3 Real-world data

Beyond these benchmark systems, we apply the product-unit model to accelerometer data from human gait. While previously differential equations were learned from state derivatives, here we use a time-delay embedding approach, i.e., predicting the next point in a trajectory directly based on multiple previous states. This creates a high-dimensional input space, as the model must consider a sequence of past measurements to capture the system's time behavior.

Human gait exhibits close to periodic behavior and is roughly sinusoidal [21, 22]. Since cosine and sine functions are solutions of linear systems of ordinary differential equations (e.g.  $\dot{x} = -y$ ;  $\dot{y} = x$ ), it is reasonable to assume that their governing equations can be captured by our approach. However, because of the noise in the data, spurious terms are to be expected.

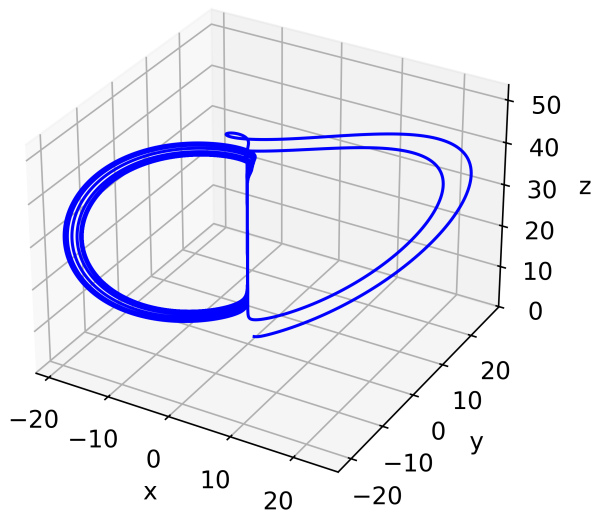


Figure 2: A simulated trajectory derived from the modified Lorenz system `Lorenz_Fract`. The structure consists of two loops of similar size, which are joined together by a narrow tube at their edges.

## 2.4 Generation of Training Data

We consider four benchmark systems and real-world human gait data. For the benchmark systems, we simulate discrete time series from the system’s equations to train the model, while the real-world data is directly measured using smartphone sensors.

### 2.4.1 Phase-Space Trajectories from Benchmark Systems

The state variables are governed by a system of ordinary differential equations as described in the previous section. The training data take the form of a discrete time series of multiple phase-space trajectories, consisting of both points  $(x, y, z)$  and their corresponding time derivatives  $\dot{x} = f_x(x, y, z)$ ,  $\dot{y} = f_y(x, y, z)$ ,  $\dot{z} = f_z(x, y, z)$ .

The points along the trajectories are generated according to the equations of the dynamical system. For each trajectory of size  $m$ , we begin by selecting an initial starting point  $p := (x, y, z) \in \mathbb{R}^3$  with coordinates drawn uniformly at random from a fixed interval. The remaining  $m - 1$  points are computed sequentially by integrating the ODEs forward using the Runge-Kutta (RK4) method. An example is shown in Fig. 3. For the trajectories for the systems `Lorenz63`, `Lorenz84`, and `Four Wing`, initial coordinates from  $[-2, 2]$  and a step size of  $\Delta t = 0.001$  are used.

Furthermore, training of the system `Lorenz_Fract` proved to be more challenging than training of other models when the range of initial values and the step size were kept the same. This could be due to the limited variation in the input. Trajectories start from a small interval and hence do not differ much at first. Moreover, the rate of divergence between two close trajectories is relatively low, as indicated by the largest Lyapunov exponent (see Sec. 2.5). Using the Python library *Lyapynov* [23], we estimate  $\lambda_{\max}$  to be approximately  $6 \times 10^{-5}$  for `Lorenz_Fract`, which is several orders of magnitude smaller than the ones of the other attractors (see Table 1).

To increase variation in the training samples for `Lorenz_Fract`, initial coordinates are drawn from a larger range, while the values of the variables  $x$ ,  $y$ , and  $z$  are constrained to non-negative numbers in the interval  $[0, 20]$  to ensure numerical stability of the RK4 integration of the fractional power. The trained model itself remains fully complex-valued and is not subject to this restriction. In addition, a larger Runge-Kutta (RK4) step size of  $\Delta t = 0.01$  is used in the construction of trajectories, allowing for a more thorough sampling of the attractor, although a smaller step size results in greater stability when integrating.

The product-unit model is then trained on multiple trajectories, with the number of trajectories ranging from 10 to 100 in increments of 10, for a total of 1000, 3000, or 5000 points, using gradient descent.

Because the trajectories are generated by simulation, their derivatives are also available. In case of real (observed) data, either numerical derivatives have to be computed first, or, as can be seen in the next section for the example of gait analysis, the current data has to be predicted directly from previous data points, as is commonly done in time-series

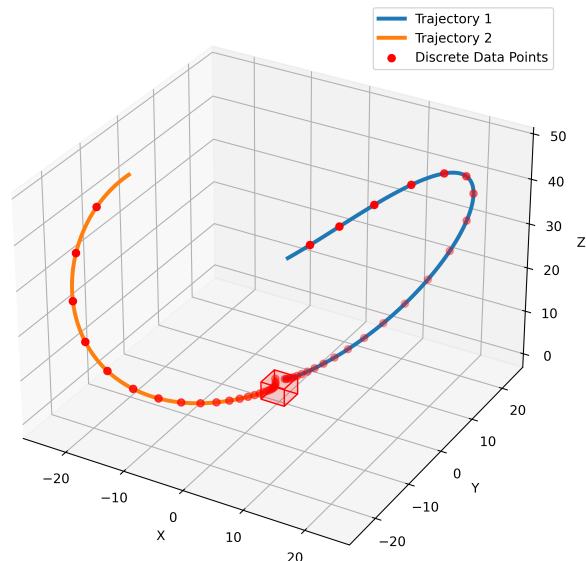


Figure 3: Two example trajectories of the Lorenz63 system, each consisting of 500 points. The initial coordinates are randomly generated within the interval  $[-2, 2]$ , as indicated by the red cube. The subsequent 499 points are computed using the fourth-order Runge-Kutta (RK4) method with a step size of  $\Delta t = 0.001$ . For clarity, only every 20th point along a trajectory is shown.

prediction. However, additional higher-order terms may arise from the described numerical procedures that are not present in the true system due to approximations. By selecting an appropriate loss function for complex-valued inputs, the model can be trained using standard backpropagation and gradient descent algorithms.

#### 2.4.2 Gait Dynamics from Wearable Accelerometers

The real-world signals are discrete observations of acceleration values along a trajectory of a walking person. The product-unit model represents a high-dimensional function that computes a current state from a sequence of previous states. Thus, a training sample consists of several points, with the subsequent point serving as the expected target, i.e.,

$$a_v(t) \approx \hat{f}_v(a(t - \psi_1), \dots, a(t - \psi_m)), \quad v \in \{x, y, z\}, \quad (8)$$

where  $a(t) = (a_x(t), a_y(t), a_z(t))$ . To capture recurring and periodic behavior, a sufficient number of time lags over an appropriate time horizon is required. Time lags are chosen according to

$$\psi_k := \lfloor 500^{k/50} + k - 1 \rfloor, \quad k = 1, \dots, m, \quad (9)$$

where  $m := 50$ . Consequently, the function lives in a 150-dimensional domain with the largest time lag equal to  $\psi_{50} = 549$ . After the model has been trained, points along a trajectory can be predicted sequentially. To improve trajectory stability, here only the real component of previous points is used to predict the next one, whereas the parameters of the model remain fully complex-valued.

To generate a signal, acceleration data are captured at a sampling rate of approximately 200 Hz using the *phyphox* app [24] on an Android device during a straight-line walk lasting 40 seconds, corresponding to 8000 data points per signal. The first 10 seconds (2000 points) of each signal are used to train the model (1451 samples). In total, ten walking time series are generated. For each time series, a model is trained and evaluated.

We used a 4th-order Butterworth low-pass filter with a cutoff frequency at 15 Hz to remove noise from the time series before using them to train the models.

### 2.5 Assessment of Model Performance for the Benchmark

After training the model, the number of identified terms—both correct and erroneous—is reported, with a margin of error allowed for any divergence from expectation. Next, the stability of subsequent trajectory predictions  $\hat{f}_x(x, y, z)$ ,  $\hat{f}_y(x, y, z)$ ,  $\hat{f}_z(x, y, z)$  is evaluated.

### 2.5.1 Counting the Number of Correctly Identified or Erroneous Terms

To compare the terms discovered by the model with the true terms, similar terms are merged and very small terms are excluded from the analysis.

After the last training iteration, the terms are merged if the exponents of the corresponding variables differ by no more than  $\epsilon = 0.1$ . Specifically, two terms  $P_j$  and  $P_k$  are merged if

$$|w_{j,i} - w_{k,i}| \leq \epsilon \text{ for all } i \in \{1, \dots, n\},$$

where  $w_{j,i}$  and  $w_{k,i}$  denote the exponents of the variable  $x_i$  in  $P_j$  and  $P_k$ , respectively. The exponents are then averaged and the coefficients summed. For example, with three-dimensional input and assuming similar exponents, two terms can be merged as

$$\begin{aligned} P_j + P_k &:= c_j x_1^{w_{j,1}} x_2^{w_{j,2}} x_3^{w_{j,3}} + c_k x_1^{w_{k,1}} x_2^{w_{k,2}} x_3^{w_{k,3}} \\ &\approx (c_j + c_k) x_1^{(w_{j,1}+w_{k,1})/2} x_2^{(w_{j,2}+w_{k,2})/2} x_3^{(w_{j,3}+w_{k,3})/2}. \end{aligned}$$

When counting correctly identified or erroneous components, we exclude terms with absolute coefficients below  $\delta = 10^{-3}$ . Predicted terms where all weights and coefficients match the true weights and coefficients with an absolute difference of at most  $\epsilon$  each are considered to be *correctly identified* terms, otherwise we call them *erroneous* terms.

### 2.5.2 Measuring Forecasting Stability

The robustness of the model can be evaluated with respect to its forecasting ability. First, in order to remove remaining noise, rounding to the third decimal place is applied to the generated system in advance. Then, to determine the predictive power of the model over a certain period of time, the effective prediction time (EPT) is calculated, as described by [8]. From the model equations, a trajectory is constructed, following the procedure described in Sec. 2.4. The initial coordinates are randomly selected from a predefined interval:  $[-4, 4]$  for Lorenz63, Lorenz84, and Four Wing, and  $[0, 40]$  for Lorenz\_Fract. Subsequent points are computed using the Runge-Kutta (RK4) method for both the true and the model system. We first integrate forward for  $5 \times 10^4$  steps by using the equations of the true system. Then, the future trajectories are generated in the same way for the true system and the predicted model and compared using the EPT. The EPT corresponds to a single point in time where a significant deviation from the expected trajectory occurs. Time is represented as a discrete sequence of consecutive steps, where  $t \in \{1, \dots, m\}$  denotes the  $t$ -th point of a simulated trajectory of size  $m$ .

The mean squared error is used for the comparison of two trajectories. The quadratic error term emphasizes large deviations at the level of individual coordinates. For complex-valued inputs, the mean squared error at time  $t$  is defined as

$$E(t) = \frac{1}{n} \sum_{i=1}^n (X_i(t) - \tilde{X}_i(t)) \overline{(X_i(t) - \tilde{X}_i(t))}. \quad (10)$$

$X$  is the time series generated from the true system and  $\tilde{X}$  denotes the time series produced by the model;  $i$  refers to the respective coordinate or axis in space.

The EPT is defined as the time elapsed before the prediction error,  $E(t)$ , exceeds a specified error threshold,  $\theta$ , for the first time. It can be formally expressed as follows:

$$EPT := \min\{t - 1 \mid t \in \{1, \dots, m\}, E(t) > \theta\}. \quad (11)$$

The error threshold  $\theta$  is chosen as the smallest standard deviation over all coordinates from the true series  $X$ .

For a dynamical system, contracting or expanding behavior can be expressed in terms of Lyapunov exponents. The largest Lyapunov exponent  $\lambda_{\max}$  quantifies the degree of exponential divergence of close trajectories in the state space [25]. The values obtained for the respective systems are shown in Table 1.

Table 1: Largest positive Lyapunov exponent per system.

Lorenz63[26]	Four Wing[20]	Lorenz84[19]	Lorenz_Fract <sup>a</sup>
0.9056	0.064	0.56	$6 \times 10^{-5}$

<sup>a</sup> Calculated with the Python library *Lyapunov* [23].

For better comparison, we normalize the EPT by the Lyapunov Time, which is the reciprocal of this value  $\frac{1}{\lambda_{\max}}$  [27], and also multiply it by the step size  $\Delta t$ . Thus, we have

$$\widehat{EPT} := EPT \times \Delta t \times \lambda_{\max}. \quad (12)$$

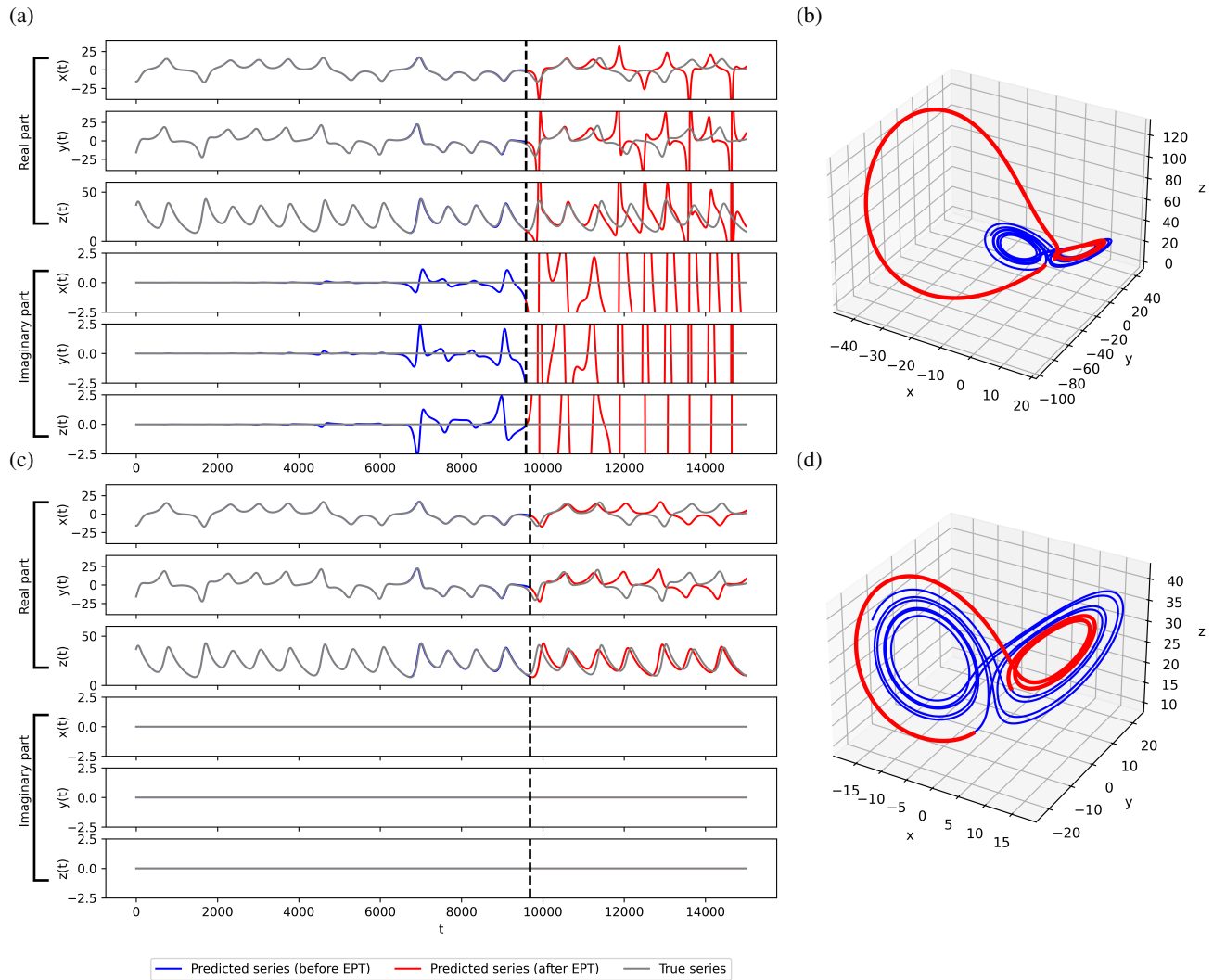


Figure 4: Effect of erroneous model parameters on the dynamic behavior of the system. (a) Comparison of simulated trajectories obtained for the true Lorenz63 system (gray line) and a corrupted Lorenz63 system (blue and red lines), using identical starting values before and after the EPT are shown. After the  $\widehat{EPT} = 8.68$  (vertical line), large deviations from the true trajectories are observed. Before the EPT at 9585 points with  $\widehat{EPT} = 8.68$ , a growing imaginary part forebodes the EPT event. (b) The real component of the predicted series in phase space, distinguishing the trajectory before the EPT (blue line) and the 2000 points following the EPT (red line) is shown. (c) When omitting the imaginary part during time series prediction, the deviations become smaller and the EPT at 9684 points with  $\widehat{EPT} = 8.77$  improves by 99 points. (d) The trajectories in phase space closely resemble the Lorenz attractor.

Fig. 4 shows an example of the EPT. A trajectory generated by the true Lorenz63 system is compared with one evolved for corrupted Lorenz63 system in which the first equation is altered as

$$\dot{x} = -10x + (10.001 + 0.001i)y, \quad (13)$$

resembling some inferences produced by our product-unit model.

Even after rounding to three decimal places, small residual imaginary parts may remain. These components also contribute to the prediction error and reduce the effective prediction time of the trajectory. Moreover, through nonlinear couplings, imaginary parts can also influence the real components of the equations. Their removal from the system after training can thus improve the stability of the trajectory evolution, as can be seen in Fig. 4. However, removing the imaginary component from the system did not substantially increase the EPT (from 8.68 to 8.77), a behavior also observed for most systems inferred by the product-unit model.

We frequently observed that changes in the imaginary parts serve as a reliable early indicator of an imminent deviation from the expected trajectory (e.g., Fig. 4a). In a previous study on nuclear mass predictions with complex product-unit networks, the imaginary component of the output was assumed to indicate prediction uncertainty [17]. For this reason, and because the EPT generally did not show significant increases without them, we do not discard the imaginary parts, aside from rounding to the third decimal place, in the simulations.

### 3 Results

We evaluate the model on four benchmark systems and subsequently apply it to real-world gait data, assessing both symbolic recovery accuracy and predictive stability. For the benchmark, we use the well-known Lorenz63 system [1], Lorenz84 [19] and Four Wing [20], each described by three coupled nonlinear ordinary differential equations. In addition, we examine a modified version of Lorenz63, Lorenz\_Fract, which contains a fractional exponent. Throughout the benchmark experiments, derivatives are treated as directly observable quantities rather than being estimated from discretely sampled states. For the gait application, the problem is substantially higher-dimensional; here, the model predicts the next state solely from a set of lagged previous observations, as analytic equations are unavailable.

The loss function is taken as the mean squared error in the following, defined for complex-valued inputs by

$$CMSE = \frac{1}{n} \sum_{i=1}^n (f_i - \hat{f}_i) \times \overline{(f_i - \hat{f}_i)}, \quad (14)$$

so that  $f_i$  denotes the true function value, while  $\hat{f}_i$  represents the prediction produced by the product-unit model. For all the dynamical systems considered, there are three state variables ( $n = 3$ ).

#### 3.1 Performance on Benchmark Systems

The training data is prepared as outlined in Sec. 2.4, for different choices of points and trajectories. The expected output for the points along a trajectory is obtained by evaluating the system’s equations at those points. This output,  $\hat{x}_i := f_i(x_1, \dots, x_n)$ , is then compared to the model’s predicted results,  $\hat{f}_i(x_1, \dots, x_n)$ , within the loss function (Eq. 14).

The parameters are kept the same across all systems, except for two changes in the generation of training data for Lorenz\_Fract (Sec. 2.4).

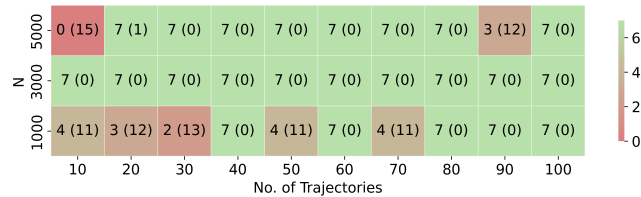
Training is performed for 5000 epochs using the Adam algorithm [28]. The initial learning rate is set to 0.03 for the coefficients and to 0.003 for the weights of the exponents, with both rates exponentially decayed by a factor of  $\gamma = 0.999$  at each epoch. The batch size is set to 30. The model uses the minimum number of product units needed to accurately represent the system. For Lorenz63 and Lorenz\_Fract, this is five; for Four Wing, six; and for Lorenz84, eight.

We count the final number of discovered terms and subsequently measure the *effective prediction time* (EPT) of the resulting system (Sec. 2.5).

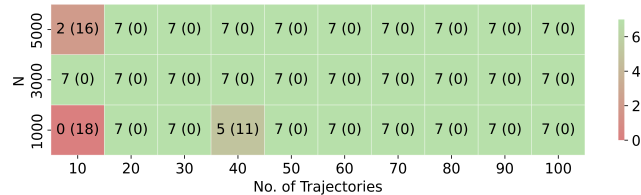
##### 3.1.1 Model discovery

We repeatedly observed a significant relationship between the number of correctly identified and erroneous terms. When not all terms were discovered, the number of erroneous terms tended to be higher. Conversely, in cases where all expected system terms were correctly identified—except for three instances in total—no erroneous terms were observed.

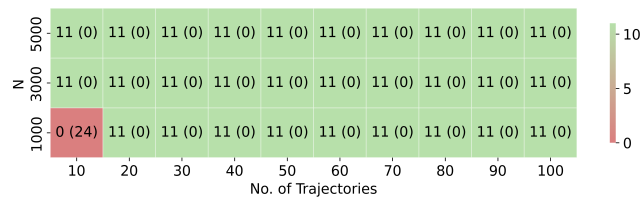
## Model discovery for dynamical systems with complex-valued product units



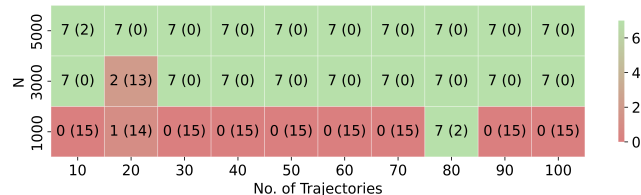
(a) Lorenz63, five product units.



(b) Four Wing, six product units.



(c) Lorenz84, eight product units.



(d) Lorenz\_Fract, five product units.

Figure 5: Heatmap of the number of correctly identified terms across different combinations of points and trajectories. The number of erroneous terms is indicated in brackets. For illustration, the minimum number of product units required is used for each system. When at least 3000 points and their derivatives are supplied for training, the model consistently identifies the precise terms and rarely introduces spurious ones.

In Fig. 5, the number of terms correctly recovered by the product-unit model is shown for the different dynamical systems and choices of points and trajectories. The number of terms identified as erroneous is reported in brackets.

The product-unit model demonstrated strong performance in representing the functions of dynamical systems. For Lorenz63, Four Wing and Lorenz84, all terms of the respective equations were correctly recovered in about 88% of the trials, across varying numbers of points and trajectories. When at least 3000 points were used for training, this proportion increased to 95%.

With the modifications to the training data outlined in Sec. 2.4, similar results to those of the other systems were obtained for Lorenz\_Fract. While 1000 points were rarely sufficient to learn the equations, 3000 points already resulted in complete representations in 9 out of 10 trials.

Apart from the choice of the optimizer or learning rate, the most relevant and challenging parameter to determine is the number of product units, which must be equal to or greater than the number of distinct monomials in the system. Note that the same units appear in each equation, differing only in their coefficients (Sec. 2.1). To obtain a minimal representation, we permit merging of terms that are sufficiently similar to one another (Sec. 2.5).

To estimate the influence of more available product units, we repeated the analysis depicted in Fig. 5 for Lorenz63 with varying choices of this parameter  $m$  in Eq. 2. A larger number of product units may offer more opportunities to correctly identify the terms, but it also increases model complexity.

Figure 6a indicates that employing slightly more product units than minimally required for term representation does not significantly alter the model’s ability to accurately identify the expressions. For the Lorenz63 system, there are seven terms in total, which can be represented with five product units. Best performance was achieved with six product units, but overall five to seven units produced similar results. With ten units, full recovery of all terms is still achieved in at least 25% of cases.

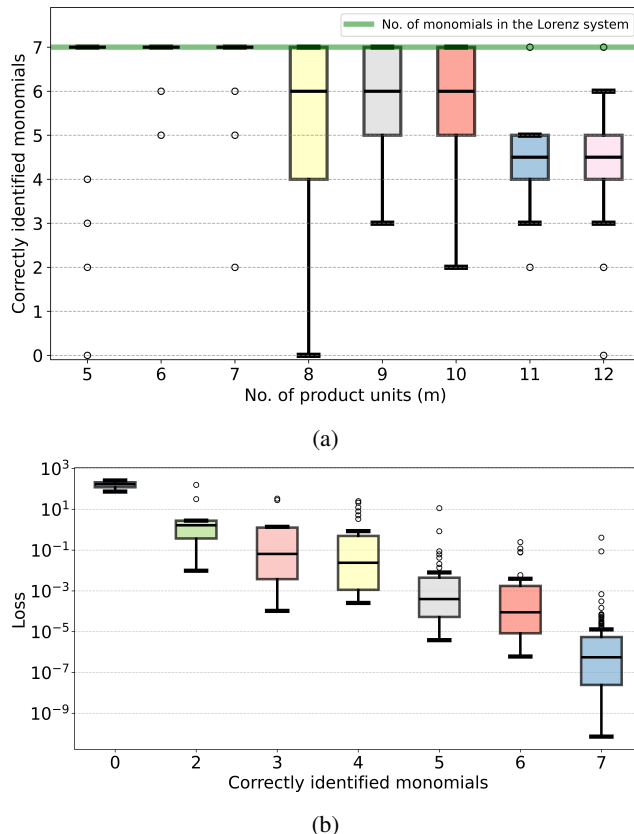


Figure 6: Dependence of the number of correctly identified terms in the Lorenz63 model on the number of product units in the network (a), and dependence of the test loss on the number of correctly identified terms (b). For 5 – 7 product units, all terms are correctly identified in at least 75% of cases, and for 8 – 10 product units in at least 25% of cases (a). The test loss is indicative of the number of correctly identified terms (b).

Furthermore, when the underlying dynamics are unknown and there is no prior expectation regarding the number of expressions involved, Figure 6b suggests that the loss can provide an indication of the number of dominant terms in the system.

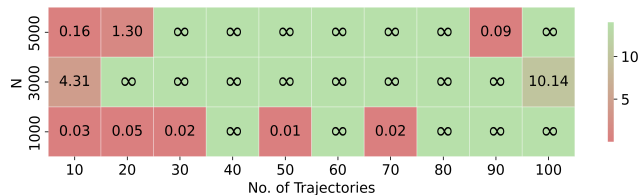
### 3.1.2 Time series prediction

Prediction of chaotic time series is often done using deep neural networks, which generally demonstrate strong performance [29, 30, 31, 32]. In a recent work using reservoir computing, more than 30 Lyapunov times could be predicted for the Lorenz system [26]. However, the black-box character of many of these approaches severely limits the interpretability of the recovered models. Moreover, extracting some of the key monomials may also improve forecasting performance, motivating the application of our method to this task [8].

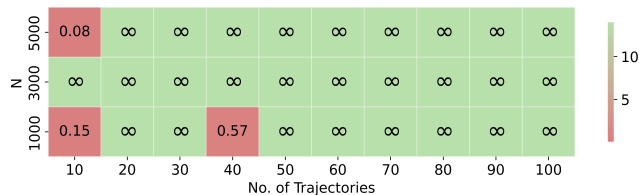
The effective prediction time (EPT) is calculated as described in Sec. 2.5. The EPT measures the elapsed time before the predicted trajectory significantly deviates from the trajectory with the same initial coordinates, but governed by the true system. As such, a higher EPT signifies more stable predictive performance. Fig. 7 shows the effective prediction time for the different dynamical systems and choices of points and trajectories. Even when all system terms are identified by our counting method, small deviations from the true equations can remain, resulting in a finite EPT.

For the product-unit model, the EPT on the benchmark systems highly depends on its ability to resolve all of the leading terms. When it failed to identify at least one of them, the resulting EPT consistently fell below one. However, with a

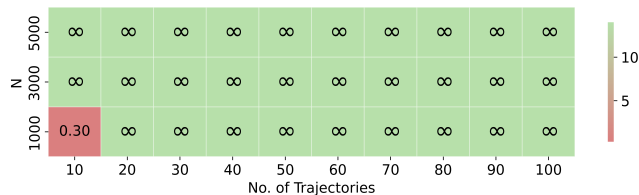
sufficient amount of training data, the produced equations were often identical to expectation, allowing the underlying dynamics to be predicted indefinitely. The exact systems of Lorenz63, Lorenz84 and Four Wing were resolved in 84% of all trials and in 90% of experiments with at least 3000 points, although a slight difference in success was observed between Lorenz63 and the other two systems of ODEs (Fig. 7a-c). Using 3000 training points for Lorenz\_Fract produced models identical to the true system in seven out of ten cases, and 5000 points increased this to nine out of ten (Fig. 7d).



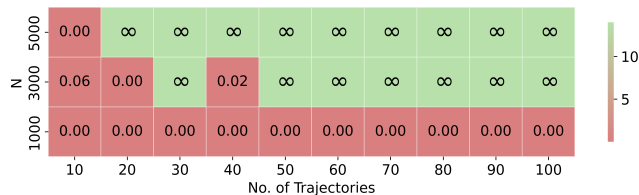
(a) Lorenz63, five product units.



(b) Four Wing, six product units.



(c) Lorenz84, eight product units.



(d) Lorenz\_Fract, five product units.

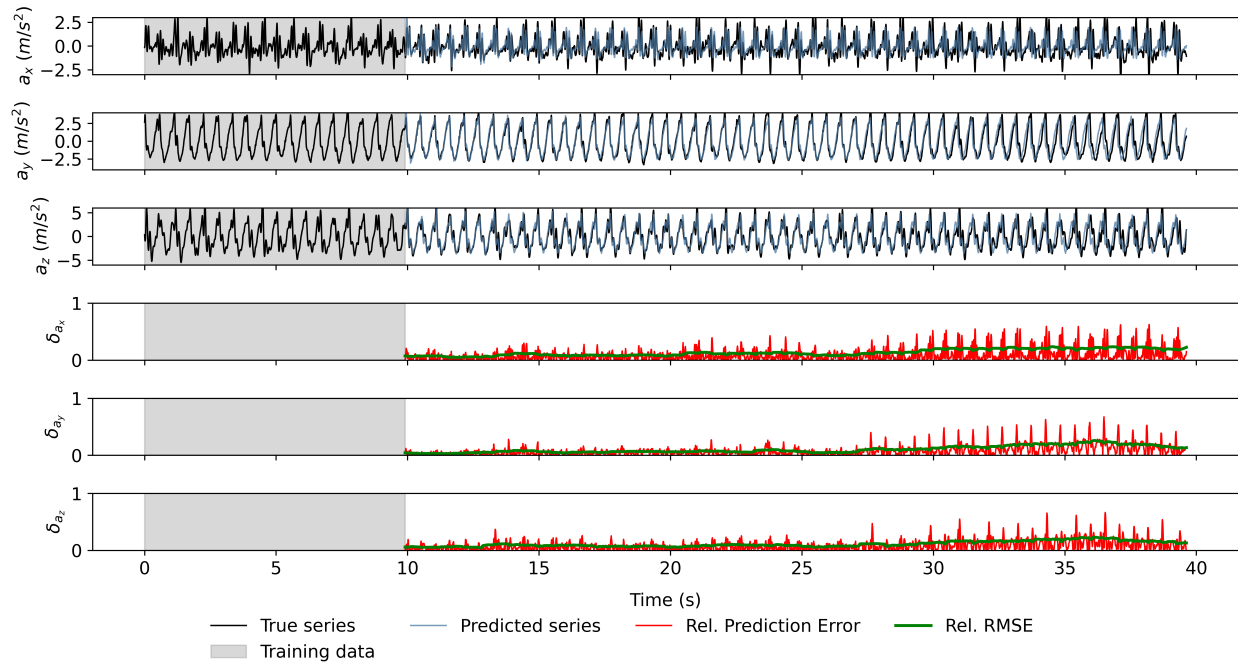
Figure 7: Heatmap of the effective prediction time for systems recovered by the product-unit model under varying training data. A high  $\widehat{EPT}$  indicates stable predictive performance. Rounding to the third decimal point is performed in advance, and this often results in the discovery of the exact equations of the system. In those cases,  $\widehat{EPT} = \infty$ , as the predicted and expected systems are indistinguishable.

### 3.2 Application to Human Gait Signals

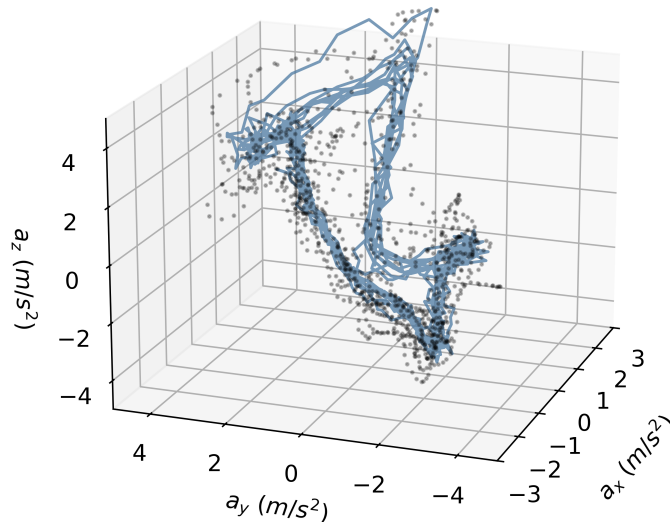
To demonstrate the model's performance on a high-dimensional system, the application to human gait analysis is explored. The problem involves a finite walking pattern signal consisting of acceleration values in three directions, with the goal of forecasting the time series behavior.

The numerous variables involved in human gait make it difficult to derive precise future predictions, but we aim to produce a stable trajectory that approximates the true signal.

As described in Sec. 2.4, we consider ten walking signals, each containing 8000 points, of which 2000 are used for training. In contrast to the benchmark instances, the next state in the acceleration time series along the  $x$ ,  $y$  and  $z$  directions is modeled as a function of 50 previous states sampled at various time lags  $\psi_k$ . In the loss function described



(a)



(b)

Figure 8: Human walking acceleration signals predicted by the product-unit model. (a) True signal trajectory (black) and product-unit model output (steel-blue) in the  $x$ ,  $y$ , and  $z$  directions. Data from the first ten seconds are used for training, as indicated by the dashed black line. The inferred system precisely predicts the further course of  $a_y$  and  $a_z$  for the considered time frame. The lower three panels show the relative prediction error  $\delta_{a_v}(t) = \frac{|a_v^{\text{true}}(t) - a_v^{\text{pred}}(t)|}{\max_t a_v(t) - \min_t a_v(t)}$  for each direction, normalized by the signal peak-to-peak range, i.e. the difference between its maximum and minimum values. The error remains bounded throughout the 30 s test interval, with a small upward trend, and inherits the periodic structure of the gait cycle. The green line in each error panel marks the moving root-mean-square error (RMSE), computed over a sliding window of approximately one second and normalized by the signal peak-to-peak range. (b) The first five seconds of the two trajectories in the 3D phase space. Strong quasi-periodic behavior is observed, as expected for a steady walking cycle.

earlier (Eq. 14), the prediction of the product-unit model,  $\hat{f}_i(a(t - \psi))$ , is thus compared against the true coordinates  $a_i(t)$  of the next point.

300 product units are used for the representation. Training is performed for 500 epochs with a batch size of 30 using the Adam algorithm. The initial learning rate is set to 0.03 for the coefficients and 0.003 for the exponent weights, with the rates decayed by  $\gamma = 0.99$  per epoch.

The product-unit model routinely captures the dynamics of the corresponding signals: Within only a few hundred epochs, the model consistently converges to a stable trajectory that provides a reasonable projection based on the training data and closely resembles the true signal for at least a few thousand data points (e.g., see Fig. 8), with one second corresponding to approximately 200 points. In some cases, the signal closely matched the expected trajectory throughout the entire time interval, although  $a_x$  proved slightly more difficult to learn due to its more complex dynamics compared to the other directions.

Quantitatively, the relative prediction error remained bounded throughout the 30 s test interval. The root-mean-square error (RMSE) is computed over the full signal and normalized by its amplitude range, defined as the difference between the maximum and minimum values

$$\widehat{\text{RMSE}}_v = \frac{\text{RMSE}_v}{\max_t a_v(t) - \min_t a_v(t)},$$

yielding a relative RMSE of approximately  $\widehat{\text{RMSE}}_x \approx 0.14$ ,  $\widehat{\text{RMSE}}_y \approx 0.12$ , and  $\widehat{\text{RMSE}}_z \approx 0.12$ . In Fig. 8, a *moving* RMSE is shown, computed over a one-second sliding window and also normalized by the full signal amplitude range. Importantly, only moderate growth of the error over time was observed, indicating that the model does not accumulate substantial drift on a horizon three times longer than the training interval.

## 4 Summary and Conclusions

This work addresses the problem of recovering the governing equations of dynamical systems directly from observed trajectory data. We proposed the complex-valued product-unit model as a library-free approach to sparse dynamical system representation, in which the relevant monomials, including those with fractional or negative exponents, are learned directly from data rather than selected from a predefined candidate set. This distinguishes the approach from established methods such as SINDy or symbolic regression, which rely on a fixed function library, while preserving the potential to obtain sparse and interpretable representations of the underlying dynamics.

The approach was evaluated on four benchmark systems of coupled ordinary differential equations: Lorenz63, Lorenz84, Four Wing, and a fractional variant of Lorenz63 (Lorenz\_Fract). In the majority of trials, the product-unit model reliably recovered the precise terms of each system. When at least 3000 training points were provided, the exact equations were identified in 90% of experiments for the integer-exponent systems, and in 70–90% of trials for Lorenz\_Fract, demonstrating that the approach extends naturally to non-integer power laws. This is of particular importance for high-dimensional problems that may consist of many different non-linear interactions, making it difficult to predefine relevant monomials before training. The recovered models, assessed via the effective prediction time (EPT), remained stable and close to the well-known attractors even beyond the EPT when the spurious imaginary terms were discarded. On the other hand, exploding imaginary components were observed close to the EPT and support earlier observations that the emergence of spurious imaginary components may serve as a useful indicator of the reliability of the predictions of product-unit networks.

The method was subsequently applied to real-world human gait signals — a substantially higher-dimensional problem in which analytic governing equations are unavailable. Rather than learning a differential equation, the model was trained in this case to predict the next state from a series of previous observations. Using a time-delay embedding formulation, the model produced stable and plausible trajectories from short training sequences, with bounded, non-divergent prediction errors over a test horizon three times longer than the training interval, demonstrating its applicability beyond controlled benchmark settings.

Several limitations of the current approach deserve attention. First, the number of product units must be specified in advance and must be at least equal to the number of dominant terms in the system. While this is a non-trivial requirement when the system structure is unknown, Fig. 6b shows that the training loss provides some indication of model adequacy. Second, the interpretability of the model degrades rapidly with dimensionality: the gait application required 300 product units with 150 exponents each, yielding about 46,000 learnable parameters — a regime in which the sparse, human-readable representation that is the primary motivation of model discovery is largely lost. Regularization strategies and systematic term-merging procedures may help recover sparsity in such settings. Third, the model’s performance on noisy data has not been systematically evaluated; the gait signals required low-pass filtering as a preprocessing step, and robustness to measurement noise remains to be studied more carefully.

Future work could address these limitations in several directions. Adaptive or penalized methods for determining the number of product units automatically would broaden the practical applicability of the approach. Extending the framework to partial differential equations, in the spirit of recent work on physics-informed learning, is another natural direction. Finally, a more systematic evaluation of the gait application, including quantitative metrics across multiple subjects and walking conditions, may open pathways for deployment in biomedical contexts. Relevant domains of application include the detection of near-fall situations or gait anomalies, e.g. connected to neurodegenerative diseases. In this setting, the straightforward implementation, the low resource requirements, and the relatively small set of hyperparameters allow training and inference on edge computing devices, an important consideration in privacy-sensitive applications.

## References

- [1] Edward N. Lorenz. Deterministic nonperiodic flow. *Journal of Atmospheric Sciences*, 20(2):130 – 141, 1963.
- [2] Sebastian F. Brandt, Babette K. Dellen, and Ralf Wessel. Synchronization from disordered driving forces in arrays of coupled oscillators. *Phys. Rev. Lett.*, 96:034104, Jan 2006.
- [3] Rozafa Koliqi, Azmath Fathima, Arpan Kumar Tripathi, Neelofar Sohi, Rajesh E. Jesudasan, and Chinmaya Mahapatra. Innovative and effective machine learning-based method to analyze alcoholic brain activity with nonlinear dynamics and electroencephalography data. *SN Comput. Sci.*, 5(1), December 2023.
- [4] Suraj Kumar Nayak, Arindam Bit, Anilesh Dey, Biswajit Mohapatra, and Kunal Pal. A review on the nonlinear dynamical system analysis of electrocardiogram signal. *Journal of Healthcare Engineering*, 2018, 2018.
- [5] Selina S. Y. Ng, J.C. Cabrera, Peter Wai-Tat Tse, Allison H. Chen, and Kwok-Leung Tsui. Distance-based analysis of dynamical systems reconstructed from vibrations for bearing diagnostics. *Nonlinear Dynamics*, 80:147–165, 2015.
- [6] Daniel Gauthier, Erik Bollt, Aaron Griffith, and Wendson Barbosa. Next generation reservoir computing. *Nature Communications*, 12:5564, 06 2021.
- [7] Steven L. Brunton, Joshua L. Proctor, and J. Nathan Kutz. Discovering governing equations from data by sparse identification of nonlinear dynamical systems. *Proceedings of the National Academy of Sciences*, 113(15):3932–3937, 2016.
- [8] Mingyu Wang and Jianping Li. Interpretable predictions of chaotic dynamical systems using dynamical system deep learning. *Scientific Reports*, 14(1):3143, Feb 2024.
- [9] Zixiang Wu, Jianping Li, Hao Li, Mingyu Wang, Ning Wang, and Guangcan Liu. Robust prediction of chaotic systems with random errors using dynamical system deep learning. *Machine Learning: Science and Technology*, 6(2):025009, apr 2025.
- [10] Hao Li, Jianping Li, Zixiang Wu, Mingyu Wang, Guangcan Liu, Ruipeng Sun, Ruize Li, Ning Wang, Houbin Song, and Shixin Zhen. Dynamics-based predictions of infinite-dimensional complex systems using dynamical system deep learning method. *Machine Learning: Science and Technology*, 6(2):025008, apr 2025.
- [11] Trent McConaghy. *FFX: Fast, Scalable, Deterministic Symbolic Regression Technology*, pages 235–260. Springer New York, New York, NY, 2011.
- [12] Markus Quade, Markus Abel, Kamran Shafi, Robert K. Niven, and Bernd R. Noack. Prediction of dynamical systems by symbolic regression. *Phys. Rev. E*, 94:012214, Jul 2016.
- [13] Richard Durbin and David E. Rumelhart. Product units: A computationally powerful and biologically plausible extension to backpropagation networks. *Neural Computation*, 1(1):133–142, 1989.
- [14] Laurens R. Leerink, C. Lee Giles, Bill G. Horne, and Marwan A. Jabri. Learning with product units. *Advances in Neural Information Processing Systems*, 7:537, 1995.
- [15] Francisco Fernández-Navarro, Maria Angeles de la Cruz, Pedro Antonio Gutiérrez, Adiel Castaño, and César Hervás-Martínez. Time series forecasting by recurrent product unit neural networks. *Neural Computing and Applications*, 29(3):779–791, 2018.
- [16] Babette Dellen, Uwe Jaekel, and Marcell Wolnitza. Function and pattern extrapolation with product-unit networks. In João M. F. Rodrigues et al., editors, *Computational Science – ICCS 2019*, pages 174–188. Springer International Publishing, 2019.
- [17] Babette Dellen, Uwe Jaekel, Paulo S.A. Freitas, and John W. Clark. Predicting nuclear masses with product-unit networks. *Physics Letters B*, 852:138608, 2024.

- [18] Adam Paszke, Sam Gross, Francisco Massa, Adam Lerer, James Bradbury, Gregory Chanan, Trevor Killeen, Zeming Lin, Natalia Gimelshein, Luca Antiga, Alban Desmaison, Andreas Kopf, Edward Yang, Zachary DeVito, Martin Raison, Alykhan Tejani, Sasank Chilamkurthy, Benoit Steiner, Lu Fang, Junjie Bai, and Soumith Chintala. Pytorch: An imperative style, high-performance deep learning library. In H. Wallach, H. Larochelle, A. Beygelzimer, F. d'Alché-Buc, E. Fox, and R. Garnett, editors, *Advances in Neural Information Processing Systems*, volume 32. Curran Associates, Inc., 2019.
- [19] S. Vannitsem and Z. Toth. Short-term dynamics of model errors. *Journal of the Atmospheric Sciences*, 59(17):2594–2604, 2002.
- [20] Zenghui Wang, Yanxia Sun, Barend Jacobus van Wyk, and et al. A 3-d four-wing attractor and its analysis. *Brazilian Journal of Physics*, 39(3):547–553, Sept 2009.
- [21] Marianna Capecci, Lucia Pepa, Federica Verdini, and Maria Gabriella Ceravolo. A smartphone-based architecture to detect and quantify freezing of gait in parkinson’s disease. *Gait & Posture*, 50:28–33, 2016.
- [22] Jang-Hee Yoo, M.S. Nixon, and C.J. Harris. Model-driven statistical analysis of human gait motion. In *Proceedings. International Conference on Image Processing*, volume 1, pages I–I, 2002.
- [23] Thomas Savary. Lyapunov, 2025.
- [24] S Staaacks, S Hütz, H Heinke, and C Stampfer. Advanced tools for smartphone-based experiments: phyphox. *Physics Education*, 53(4):045009, may 2018.
- [25] Vasilij D. Pechuk, Tatyana S. Krasnopolskaya, and Evgeniy D. Pechuk. Maximum lyapunov exponent calculation. In Christos H. Skiadas and Yiannis Dimotikalos, editors, *14th Chaotic Modeling and Simulation International Conference*, pages 327–335, Cham, 2022. Springer International Publishing.
- [26] Lauren A Hurley and Sean E Shaheen. Reservoir computing with large valid prediction time for the lorenz system, 2025.
- [27] Boris P. Bezruchko. *Extracting knowledge from time series: an introduction to nonlinear empirical modeling*. Springer complexity. Springer, 2010. Print version record.
- [28] Diederik P. Kingma and Jimmy Ba. Adam: A method for stochastic optimization, 2017.
- [29] Pantelis R. Vlachas, Wonmin Byeon, Zhong Y. Wan, Themistoklis P. Sapsis, and Petros Koumoutsakos. Data-driven forecasting of high-dimensional chaotic systems with long short-term memory networks. *Proceedings of the Royal Society A: Mathematical, Physical and Engineering Sciences*, 474(2213):20170844, May 2018.
- [30] A. Chattopadhyay, P. Hassanzadeh, and D. Subramanian. Data-driven predictions of a multiscale lorenz 96 chaotic system using machine-learning methods: reservoir computing, artificial neural network, and long short-term memory network. *Nonlinear Processes in Geophysics*, 27(3):373–389, 2020.
- [31] Hyojung Choi, Chanhwi Jung, Taein Kang, Hyunwoo J. Kim, and Il-Youp Kwak. Explainable time-series prediction using a residual network and gradient-based methods. *IEEE Access*, 10:108469–108482, 2022.
- [32] Chuan Chen, Rui Li, Lin Shu, Zhiyu He, Jining Wang, Chengming Zhang, Huanfei Ma, Kazuyuki Aihara, and Luonan Chen. Predicting future dynamics from short-term time series using an anticipated learning machine. *National Science Review*, 7(6):1079–1091, 02 2020.